Research Square

Preprints are preliminary reports that have not undergone peer review.
They should not be considered conclusive, used to inform clinical practice,
or referenced by the media as validated information.

Performance Optimization of Tin-Based Inverted Planar Perovskite Solar Cells: Insights into Defect Density, Thickness, Absorber Concentration, and Thermal Effects via Numerical Simulation

Jonathan Terseer Ikyumbur
Benue State University
Linus Friday Apeh
fridayapeh729@yahoo.com

Benue State University
Frederick Gbaorun
Benue State University
Raymond Msughter Agaku
Benue State University
Samuel Omenka Ode
Benue State University

Research Article

Keywords: MASnI3, Inverted planar perovskite solar cells, Defect density optimization, Temperature effects, SCAPS-1D, Numerical simulation

Posted Date: May 20th, 2026

DOI: https://doi.org/10.21203/rs.3.rs-9701383/v1

License: This work is licensed under a Creative Commons Attribution 4.0 International License.
Read Full License

Additional Declarations: No competing interests reported.

Performance Optimization of Tin-Based Inverted Planar Perovskite Solar Cells. Insights into Defect Density, Thickness, Absorber concentration, and Thermal Effects via Numerical Simulation

Jonathan Terseer Ikyumbur[1] (jikyumbur@bsum.ng), Linus Friday Apeh[1](fridayapeh729@yahoo.com), Frederick Gbaorun[1](fredgbaorun@gmail.com) , Raymond Msughter Agaku[1] (agakuray@gmail.com), Ode Samuel Omenka[1] (soode@bsum.edu.ng)

[1]Department of Physics. Fr Moses Orshio Adasu University, Makurdi, Benue State, Nigeria.

Corresponding author: Jonathan Terseer Ikyumbur* (jikyumbur@bsum.ng)

Abstract

Tin-based inverted planar perovskite solar cells (IPSCs) have emerged as promising lead-free alternatives for next-generation photovoltaic technologies due to their environmental compatibility and excellent optoelectronic properties. However, their performance is still constrained by defect-assisted recombination, suboptimal layer thickness, non-ideal absorber doping, and thermal instability. In this study, a comprehensive coupled optimization of a Tin-based IPSC is performed using SCAPS-1D simulation. with particular emphasis on the role of Mg-doped TiO_2 as an electron transport layer (ETL). The device structure FTO/Cu_2O/$MASnI_3$/Mg-TiO_2/Ag is systematically optimized by examining the effects of absorber thickness, defect density, doping concentration, and operating temperature. The results demonstrate that improved band alignment and suppressed interfacial recombination at the absorber/ETL interface play a critical role in enhancing device performance. An optimal power conversion efficiency of 28.88% is achieved, corresponding to an open-circuit voltage of 0.9786 V, a short-circuit current density of 33.58 mA/cm², and a fill factor of 87.85%. Furthermore, critical thresholds for bulk and interface defect densities are identified, providing practical design guidelines for achieving high-efficiency tin-based perovskite solar cells. These findings highlight the effectiveness of Mg-doped TiO_2 in improving charge transport and device stability, offering valuable insights for the development of efficient and environmentally friendly perovskite photovoltaics.

Keywords: $MASnI_3$; Inverted planar perovskite solar cells; Defect density optimization; Temperature effects; SCAPS-1D; Numerical simulation

1. Introduction

The swift progress in the development of perovskite solar cells (IPSCs) has established them as one of the most promising photovoltaic technologies in contemporary applications. Perovskites comprise a class of compounds characterized by the general formula ABX_3, where A is usually an inorganic or organic cation (Cs^+, $CH_3NH_3^+$or $CH(NH_2)_2$), B is a metal cation (Pb^{2+}, Bi^{2+}, Ge^{2+}), and X is a halogen anion (I^-, Br^-or Cl^-). The arrangement is ionic, with BX6 creating an octahedral shape where the B atom is central, while the X atoms are connected to the corners of the cube surrounding B. This configuration is tetragonal and encompasses an octahedral structure (Fan et al., 2022). The most commonly used component as the active layer is $CH_3NH_3PbI_3$, referred to as $MAPbI_3$, or methyl ammonium lead iodide. However, perovskites based on $MAPbI_3$ are toxic because of the presence of Pb, which makes them unsuitable for commercial production (Obada et al., 2024; Ru et al., 2020).

An alternative approach involves utilizing a perovskite material composed of tin (Sn) instead of lead (Pb), specifically referred to as methylammonium tin iodide ($CH_3NH_3SnI_3$ or $MASnI_3$). Many researchers (Islam et al., 2024; Prasangi & Srilalitha, 2025; Sharif et al., 2023) have developed cells based on $CH_3NH_3SnI_3$, and this is also intended to be used in this study. Tin occurs naturally and has similar electronic properties as lead (Pb). Most importantly, Sn-based perovskite solar cells (PSCs) exhibit a narrow direct bandgap of 1.3eV, high charge mobility, exhibiting robust absorbance within the visible light spectrum coupled with exceptional bipolar charge transport characteristics, which contribute to enhanced solar cell efficiency (Durodola et al., 2023; Sumona et al., 2024).

Inverted planar PSCs, valued for their low hysteresis and ease of fabrication, still face limitations due to inefficiencies in charge transport and recombination, intrinsic defect densities, and sensitivity to temperature variations. which limit the device performance (Nyiekaa et al., 2024). Given the need for efficient, low-cost solar cells, understanding the underlying device physics and optimizing structural parameters is essential. Numerical simulation tools such as SCAPS-1D are invaluable for predicting device performance, identifying limiting mechanisms, and guiding

experimental optimization which aid in rapid and cost-effective screening of material parameters, thereby reducing experimental workload and resource consumption.

Although several simulation studies have been reported (Islam et al., 2024; Prasangi & Srilalitha, 2025; Sharif et al., 2023) on the performance optimization of Sn-based PSCs, a comprehensive and unified approach that simultaneously examine thickness optimization, defect density effects, operating temperature, and absorber doping concentration within a single inverted $MASnI_3$ device framework remains limited. Many existing works investigate these parameters in isolation. This motivates the present study.

In this work, a comprehensive coupled optimization of a Tin-based inverted planar perovskite solar cell (IPPSC) is performed using SCAPS-1D simulation. to systematically investigates the interplay between thicknesses of the absorber and hole transport layers, the density of bulk defects within the absorber, the concentration of impurity in the absorber, and the operational temperature and how these factors influence the performance metrics of $MASnI_3$-based inverted planar perovskite solar cells. The aim of this study is to clarify the dominant physical mechanisms governing device performance and to provide practical design guidelines for improving the efficiency and stability of lead-free IPSCs.

2 Theoretical framework

2.1 Poisson Equation

The electrostatic potential ψ(x) in the device is governed by the Poisson equation: given by

$$\frac{d^2}{dx^2}\psi(x) = \frac{q}{\varepsilon_0 \varepsilon_r}\left[\rho(x) - n(x) + N_D + N_A + \rho_\rho - \rho_n\right] \quad (1)$$

Where $n(x)$ and $p(x)$ are charge carrier densities of electrons and holes; the relative permittivity is ε_r, the permittivity of free-space is ε_0; N_D and N_A are the donor and acceptor impurities; the distributions of holes and electrons are ρ_ρ and ρ_n, respectively; q is the electric charge.

2.2 Continuity Equations

The density gradients, current densities, and overall generation of free charge carriers, namely electrons and holes, are governed by a continuity equation. These relationships are articulated in equations (2) and (3), which respectively describe the conservation principles at play.

$$\frac{\delta n}{\delta t} = \frac{1}{q}\frac{\partial J_n}{\partial x} + (G_n - R_n) \quad (2)$$

$$\frac{\delta \rho}{\delta t} = \frac{1}{q}\frac{\partial J_\rho}{\partial x} + (G_\rho - R_\rho) \quad (3)$$

where G_n is the generation rate, R_n is the recombination, J_n is the electron density, and J_p is the density of holes.

2.3 Drift–Diffusion Current Equations

The total current resulted by drift and diffusion of charge carriers, which can be used to obtain the current densities of the solar cell are given by

$$J_n = q\mu_n n\mathcal{E} + qD_n\delta n \quad (4)$$

$$J_p = q\mu_p p\mathcal{E} + qD_p\delta p \quad (5)$$

where μ_n is the mobility of the electron; μ_ρ is hole mobility;D_n is the coefficient of diffusion of electrons; and D_ρ is the coefficient of diffusion for the hole is contingent upon the mobility of both the hole and the electron, and it is further influenced by the carrier's lifetime. These diffusion coefficients are fundamentally connected to the dynamism of charge carriers within the medium. (Nyiekaa et al., 2024; Sumona et al., 2023).

3. Materials and methods

The inverted planar perovskite solar cell (IPSC) investigated in this study adopts a p–i–n architecture with the configuration FTO/Cu_2O/$MASnI_3$/Mg-TiO_2/Ag. The schematic diagram of the device structure is shown in Figure 4a with fluorine-doped tin oxide (FTO) as the transparent conducting front electrode, enabling efficient light transmission into the device while also serving as an electrical contact. Silver (Ag) as the back electrode due to its high electrical conductivity and suitable work function for efficient charge collection. Copper(I) oxide (Cu_2O) is employed as the hole transport material (HTM). The selection of Cu_2O is motivated by its advantageous material properties, including high intrinsic hole mobility, a relatively high absorption coefficient, and favorable valence band alignment with the absorber layer. In addition, Cu_2O is an inorganic semiconductor that is significantly more cost-effective than many commonly used organic HTMs, while also offering superior photochemical and thermal stability and good long-term stability

under ambient conditions (Prasangi & Srilalitha, 2025).These characteristics make Cu_2O a promising candidate for stable and scalable perovskite solar cell applications.

The absorber layer consists of methylammonium tin iodide ($CH_3NH_3SnI_3$), a lead-free perovskite material that has attracted significant research interest due to its environmental compatibility and potential for large-scale photovoltaic deployment (Abate, 2023).$CH_3NH_3SnI_3$ exhibits excellent optoelectronic properties, including a direct band gap of approximately 1.3 eV, high absorption coefficient, and efficient charge transport characteristics, making it well suited for solar energy conversion (A. Kumar et al., 2021)

Magnesium-doped titanium dioxide (Mg-TiO_2) is utilized as the electron transport material (ETM). The incorporation of magnesium improves the electronic properties of TiO_2 by enhancing its conductivity and optimizing the alignment of the conduction band with the perovskite absorber, which plays a crucial role in enhancing electron extraction efficiency while concurrently mitigating interfacial recombination processes. This interplay ultimately contributes to the superior performance of the device (Chowdhury et al., 2023).

Overall, the selected materials and device architecture provide favorable band alignment, efficient charge transport pathways, and improved stability, making the proposed structure suitable for investigating the performance of tin-based inverted planar perovskite solar cells.

The simulations of the device were conducted utilizing the Solar Cell Capacitance Simulator (SCAPS-1D), a sophisticated tool that numerically resolves the core equations governing semiconductor behavior. This includes the application of Poisson's equation in conjunction with the continuity equations for both electrons and holes, employing an iterative methodology for enhanced accuracy. By incorporating the specified material properties and interface parameters, the simulator generates key device characteristics such as the current density–voltage (J–V) curve, energy band alignment, recombination profiles, and external quantum efficiency. From these outputs, the principal photovoltaic parameters, including open-circuit voltage (V_{OC}), short-circuit current density (J_{SC}), fill factor (FF), and power conversion efficiency (PCE) are extracted(Patel, 2021).

The simulations were performed under standard test conditions with an illumination intensity of 1000 W/m² corresponding to the AM 1.5G solar spectrum. The operating temperature was varied

from 300 K to higher temperatures in order to evaluate the thermal stability and performance sensitivity of the device. In addition, the series and shunt resistances were systematically adjusted to investigate resistive loss mechanisms within the cell. The work function of the front contact, fluorine-doped tin oxide (FTO), was set to 5.0 eV, while that of the back contact, silver (Ag), was taken as 4.3 eV. The material parameters utilized in this investigation were meticulously curated based on established theoretical frameworks, empirical observations, and previously published literature, and are encapsulated in Table 1. Conversely, the parameters at the interface are detailed in Table 2. The simulation incorporated neutral defect states, which were characterized as non-reactive defects that neither donate nor accept charge carriers within the bulk layers or at the interfaces. In addition, the densities of bulk defects were deliberately selected to exceed ideal values marginally, thereby enhancing the fidelity of the model to reflect realistic experimental conditions and the constraints inherent in practical device fabrication.

In this investigation, specific parameters such as electron mobility, hole mobility, carrier diffusion length, and interfacial resistance were posited to remain invariant and were derived from authoritative sources in the existing literature. These parameters are strongly influenced by fabrication techniques and experimental conditions, and their variability can substantially affect the real-world performance of perovskite solar cells. Fixing these parameters allows the study to focus on the specific variables under investigation while maintaining consistency with previously reported results. In practical device fabrication, discrepancies between simulated and experimental performance may arise from several factors, such as variations in relative humidity and temperature, differences in measurement equipment and calibration, procedural inconsistencies, operator expertise, and the degree of control over crystallization dynamics and grain growth during film formation. These factors collectively influence the microstructure and electronic quality of the materials, thereby affecting overall device efficiency and stability.

Table 1. Details of the input data for the perovskite solar cell simulation were adopted from (Islam et al., 2024; Mallahasan & Onay, 2022; Nyiekaa et al., 2024; Patel, 2021; Usman & Bovornratanaraks, 2024) (Nyinongo et al., 2025)(Gholami-Milani et al., 2023)

Parameter	Cu_2O	$CH_3NH_3SnI_3$	Mg-TiO_2
Thickness(μm)	0.05	0.45	0.019
bandgap, (eV)	2.1	1.3	3.22

electron affinity, (eV)	3.2	4.2	4.2
dielectric permittivity, ε_r	7.6	10.0	13.6
CB effective density of states, N_C (cm $^{-3}$)	2.0×10^{18}	1×10^{18}	2.20×10^{18}
CV effective density of states, N_V (cm $^{-3}$)	1.0×10^{19}	1×10^{19}	2.0×10^{19}
electron mobility, μ_n (cm^2 V^{-1} S^{1-})	20	2000	2.0×10^{1}
hole mobility, μ_p (cm^2 V^{-1} S^{1-})	80	300	1.0×10^{1}
acceptor density, N_A (cm $^{-3}$)	1×10^{17}	3.2×10^{15}	0.0
donor density, N_D (cm $^{-3}$)	0.00	0.00	9.0×10^{20}
defect density, N_t (cm $^{-3}$)	1×10^{14}	1×10^{15}	1×10^{15}

Table 2. Data for interface layers

Parameter	$Cu_2O/CH_3NH_3SnI_3$	$CH_3NH_3SnI_3/Mg\text{-}TiO_2$
Defect type	Neutral	Neutral
capture cross section for electrons(cm^{-2})	1×10^{-15}	2×10^{-15}
Capture cross-section for hole(cm^{-2})	1×10^{-15}	2×10^{-15}
Energetic distribution	Single	Single
Energy level with respect to Ev (ev)	0.60	0.60
Characteristic energy(ev)	0.1	0.1
Total density (cm^{-3})	1×10^{10}	1×10^{10}

4. Results and Discussion

Upon exposure to light, photons absorbed in the $MASnI_3$ layer induce the formation of electron–hole pairs. The presence of an intrinsic electric field within the device facilitates the movement of electrons toward the electron transport layer ($Mg\text{-}TiO_2$), while holes are directed toward the hole transport layer (Cu_2O). This effective separation and subsequent collection of charge carriers at

their designated electrodes result in the generation of photocurrent and photovoltage within the apparatus.

The baseline performance of the inverted planar perovskite solar cell with the structure FTO/Cu_2O/$MASnI_3$/Mg-TiO_2/Ag was first evaluated using the initial parameters summarized in Tables 1 and 2. The simulated current density–voltage (J–V) characteristics of the unoptimized device are presented in Figure 2a. The device exhibited an open-circuit voltage (VOC) of 0.8878 V, a short-circuit current density (JSC) of 30.45 mA/cm², a fill factor (FF) of 82.21%, and a power conversion efficiency (PCE) of 22.23%. These findings substantiate the capability of the proposed architecture to attain competitive photovoltaic performance, even in the absence of optimization efforts.

The external quantum efficiency (EQE) spectrum of the device is presented in Figure 3. The device demonstrates a robust photoresponse throughout the visible spectrum (300–900 nm), achieving a peak quantum efficiency near 98% at approximately 580 nm. This elevated spectral response underscores the effective photon absorption and charge collection mechanisms within the absorber layer, aligning with findings previously documented for $MASnI_3$-based perovskite solar cells (Zhou et al., 2024)(Totolhua et al., 2023)(Rengifo-Herrera et al., 2022). To optimize device performance, a systematic investigation was conducted on several key parameters, specifically the thickness of the absorber layer, the thickness of the hole transport layer (HTL), the bulk defect density within the absorber, the doping concentration, and the operating temperature. These parameters are pivotal in influencing charge transport dynamics, minimizing recombination losses, and ultimately enhancing the overall efficiency of the device. The photovoltaic metrics PCE, V_{OC}, J_{SC}, and FF were used as evaluation criteria to determine the optimal conditions.

Following the optimization process, a significant improvement in device performance is displayed in Figure 2b. The optimized device with the configuration FTO/Cu_2O/$MASnI_3$/Mg-TiO_2/Ag achieved a PCE of 28.88%, with a V_{OC} of 0.9786 V, J_{SC} of 33.58 mA/cm², and FF of 87.85%

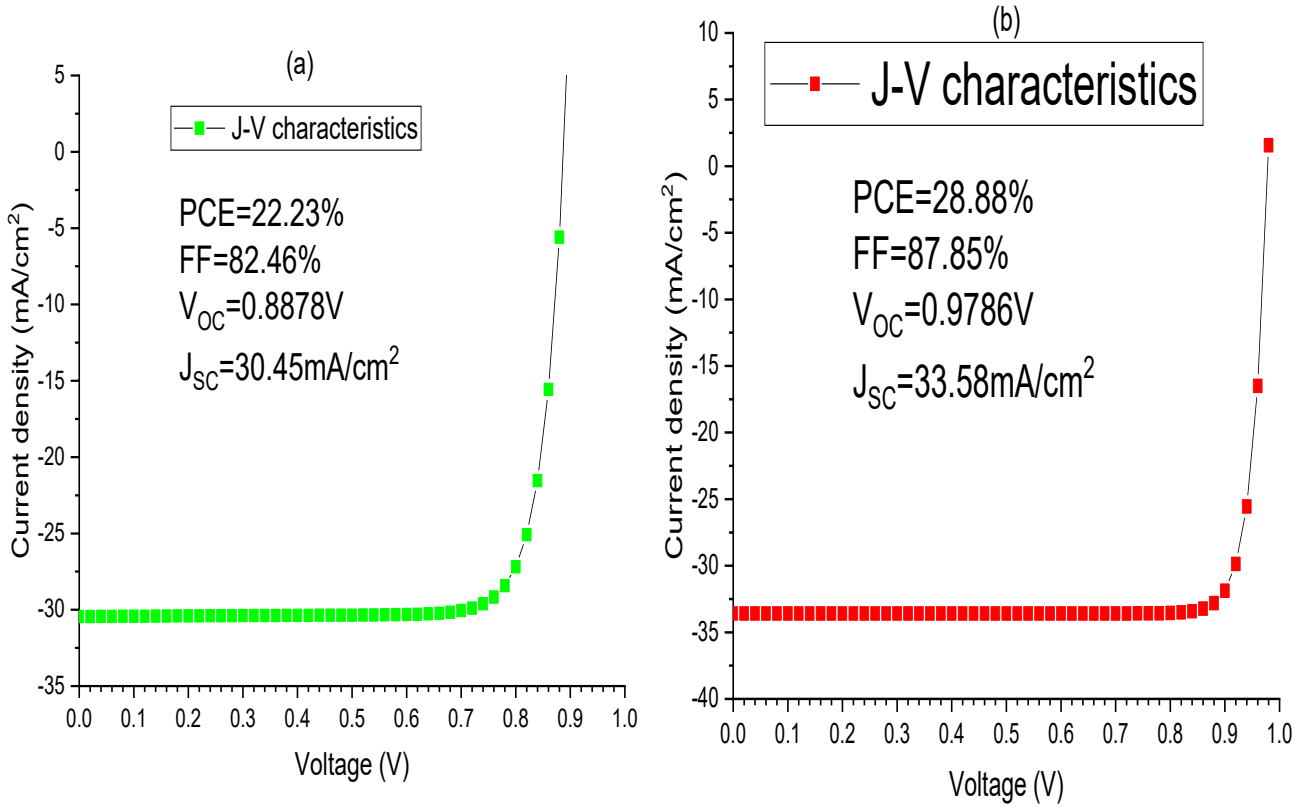


Figure 2. J-V characteristics of the (a) unoptimized and (b) optimized device using $MASnI_3$ as absorber, Mg-TiO_2 as ETM, Cu_2O as HTM, FTO as front contact, and Ag as back contact, respectively.

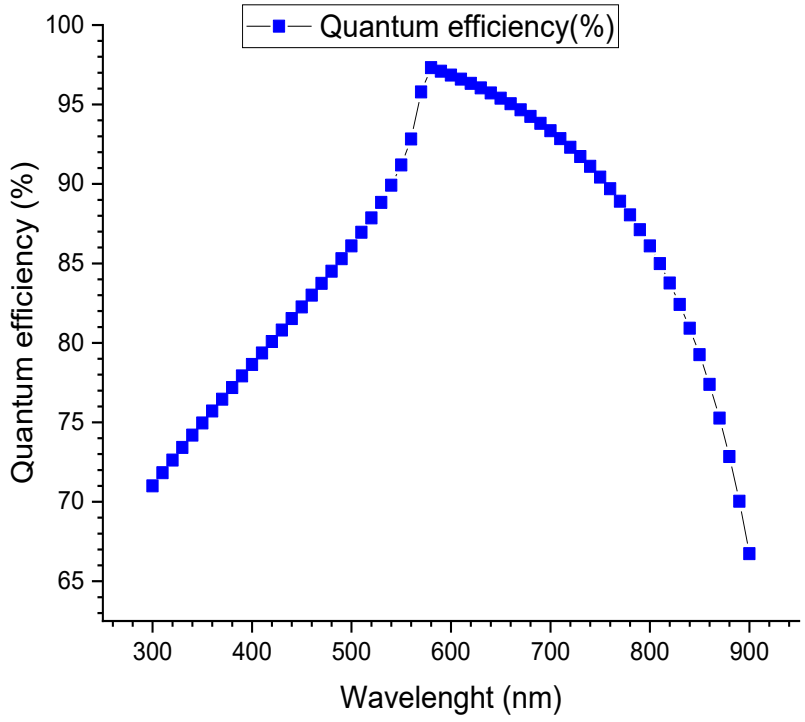


Figure 3. Quantum efficiency of the proposed inverted perovskite solar cell

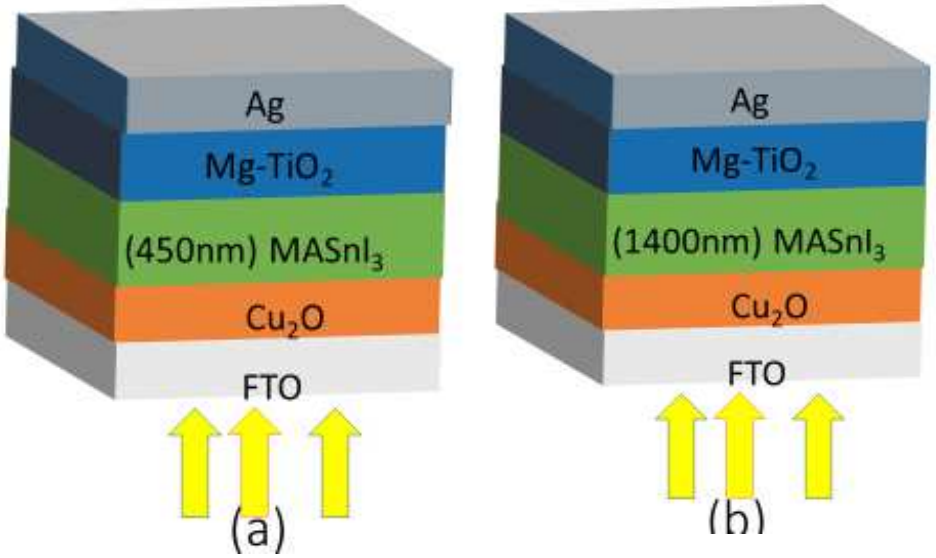


Figure 4: Schematic Representation of the (a) unoptimized and (b) optimized device.

4.1. Effect of Absorber Layer Thickness on IPSC

The impact of the absorber layer thickness on the efficacy of IPSCs was rigorously investigate by varying the thickness from 0.4 µm to 1.6 µm. The relevant photovoltaic parameters are encapsulated in Table 3, while the relationships among power conversion efficiency (PCE), fill factor (FF), open-circuit voltage (V_{OC}), and short-circuit current density (JSC) as functions of absorber thickness are illustrated in Figure 5.

The results demonstrate that absorber thickness strongly affects charge generation, transport, and recombination dynamics. Increasing the absorber thickness enhances photon absorption, particularly in the long-wavelength region, which leads to a higher short-circuit current density. Specifically, J_{SC} increases from 29.7 mA/cm² at 0.4 µm to 33.7 mA/cm² at 1.2 µm, reflecting improved photo carrier generation and collection. At very low thicknesses (0.4 µm), insufficient absorption limits the generation of electron–hole pairs, resulting in a lower photocurrent despite a higher V_{OC}, which indicates reduced recombination in thinner layers (Bouderbala & Hamdi, 2023).

With an increase in absorber thickness, there is a progressive decline in the open-circuit voltage, which can be attributed to heightened bulk recombination processes. Conversely, the fill factor experiences an enhancement, driven by more effective charge extraction mechanisms and a reduction in series resistance losses. The external quantum efficiency (EQE) of the device also benefits from thicker absorber layers, as the effective band gap decreases slightly, allowing absorption of longer-wavelength photons and thereby increasing the overall photo-generated current (Li et al., 2022). The study identifies an optimal absorber thickness range of 1.2–1.4 μm. At 1.4 μm, the device achieves its maximum PCE of 23.7%, representing an improvement of approximately 1.9% compared to the 0.4 μm device. Beyond this thickness, the efficiency plateaus and eventually declines. This behavior occurs because light absorption reaches near-saturation, as evidenced by the nearly constant J_{SC} values, and because charge carriers generated deep within the absorber exceed the carrier diffusion length, leading to increased recombination losses (Sumona et al., 2024)

These results highlight the significant influence of absorber thickness on the studied phenomena in balancing photon absorption, charge extraction, and recombination dynamics. For $MASnI_3$-based IPSCs, controlling the absorber thickness within the range of 1.2–1.4 μm provides a practical guideline for maximizing device efficiency while avoiding the adverse effects associated with overly thick layers.

Table 3. J-V characteristic parameters with the variation of the thickness of the Absorber layer

Thickness (μm)	PCE(%)	FF(%)	J_{SC}(mA/cm^2)	V_{OC}(V)
0.4	21.8	82.1	29.7	0.892
0.6	23.0	82.3	31.8	0.876
0.8	23.4	82.8	32.7	0.865
1.0	23.6	83.0	33.2	0.856
1.2	23.7	83.4	33.5	0.848
1.4	23.7	83.6	33.6	0.843
1.6	23.7	83.8	33.7	0.838

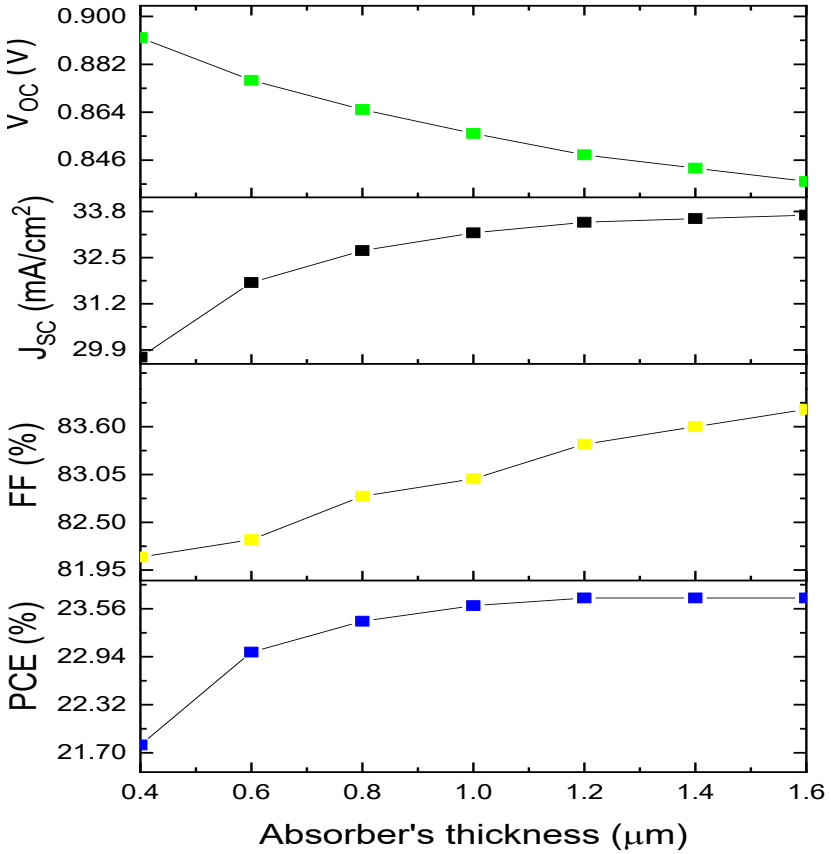


Figure 5. Plots of PCE, FF, $J_{SC,}$ and V_{OC} against the thickness of the Absorber layer

4.2. Effect of Acceptor Doping Concentration of the Absorber Layer (N_A)

In addition to absorber thickness, the acceptor (hole) doping density of the $MASnI_3$ absorber layer plays a critical role in determining the performance of inverted planar perovskite solar cells (Usman & Bovornratanaraks, 2024). Table 4 summarizes the impact of varying the acceptor concentration (NA) on the Fermi energy level and photovoltaic parameters. As the concentration of acceptor dopants escalates, the Fermi level associated with holes experiences a downward shift, resulting in an elevation of the open-circuit voltage (VOC), as depicted in Figure 6. This phenomenon can be ascribed to the intensified built-in electric field that arises from augmented acceptor densities. Such an enhancement facilitates more effective charge separation while simultaneously mitigating recombination losses.

In this study, the acceptor concentration of the absorber layer was varied from 1×10^{12} cm^{-3} to 1×10^{16} cm^{-3} to identify the optimal value for device performance. The simulation results indicate that both V_{OC} and fill factor (FF) increase with higher doping concentration, leading to an overall improvement in power conversion efficiency (PCE). At the highest simulated concentration of 1×10^{16} cm^{-3}, the device exhibits the best performance with V_{OC}= 0.912 V, J_{SC} = 30.30 mA/cm², FF = 84.5%, and PCE = 23.4% (Figure 6).

Concurrently, the short-circuit current density (JSC) exhibits a subtle reduction as the NA rises. This slight decline may be primarily ascribed to enhanced carrier recombination within the absorber layer or a potential increase in series resistance associated with elevated doping levels (Oni et al., 2024). Overall, the results highlight that careful tuning of the absorber layer's acceptor concentration is essential to achieve optimal device performance, balancing enhanced V_{OC} and FF against minimal losses in J_{SC}.

Table 4. J-V characteristic with variation of acceptor density (N_A) of the Absorber layer

$N_A(cm^{-3})$	PCE(%)	FF(%)	$J_{SC}(mA/cm^2)$	$V_{OC}(V)$
1×10^{12}	22.1	81.8	30.5	0.887
1×10^{13}	22.1	81.8	30.5	0.887
1×10^{14}	22.1	81.9	30.5	0.887
1×10^{15}	22.2	82.2	30.5	0.888
1×10^{16}	23.4	84.5	30.3	0.912

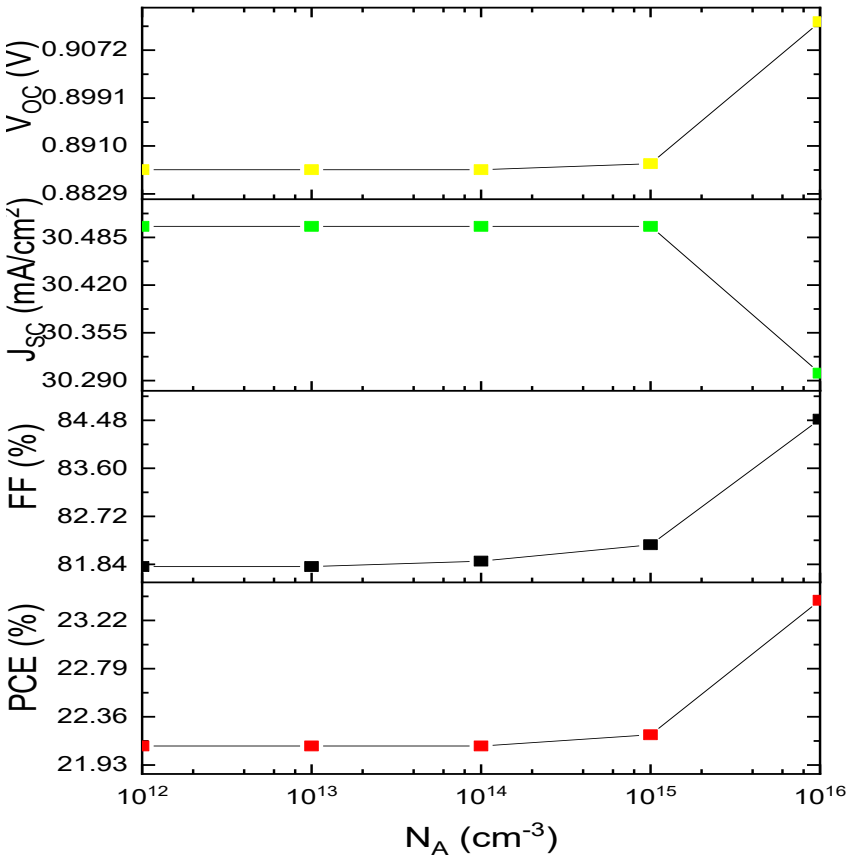


Figure 6. Plots of PCE, FF, $J_{SC,}$ and V_{OC} against acceptor density (N_A) of the absorber lay

4.3 Effect of Absorber Layer Defect Density on IPSC Device

The impact of defect density within the absorber layer on the efficacy of methylammonium tin iodide ($MASnI_3$)-based IPSCs was systematically analyzed by manipulating defect densities ranging from 1×10^{13} to 1×10^{17} cm^{-3}. The resultant photovoltaic parameters are compiled in Table 5, while the dependencies of power conversion efficiency (PCE) and fill factor (FF) on defect density are illustrated in Figure 7. Additionally, the current-voltage (J–V) characteristics at various defect density levels are depicted in Figure 7.

As evident from Table 5 and Figure 7, increasing the defect density results in a pronounced decline in PCE, FF, and V_{OC}, whereas J_{SC} remains relatively constant. The reduction in VOC with increasing defect density is attributed to enhanced Shockley–Read–Hall recombination, which

reduces carrier lifetime and quasi-Fermi level splitting (Oni et al., 2024). These results highlight that minimizing bulk defects in the absorber layer is crucial for maintaining efficient charge transport and reducing recombination losses.

Based on the simulations, an absorber defect density of 1×10^{13} cm^{-3} was identified as optimal, producing the highest device performance and demonstrating the importance of defect engineering in the design of high-efficiency $MASnI_3$-based IPSCs.

Table 5. The effect of defect density of the absorber layer on PSCs' performance characteristics.

$N_t(cm^{-3})$	PCE(%)	FF(%)	$J_{SC}(mA/cm^2)$	$V_{OC}(V)$
1×10^{13}	25.2	86.5	30.5	0.956
1×10^{14}	24.4	84.9	30.5	0.945
1×10^{15}	22.2	82.2	30.5	0.888
1×10^{16}	19.4	79.8	30.5	0.800
1×10^{17}	16.5	76.9	30.4	0.704

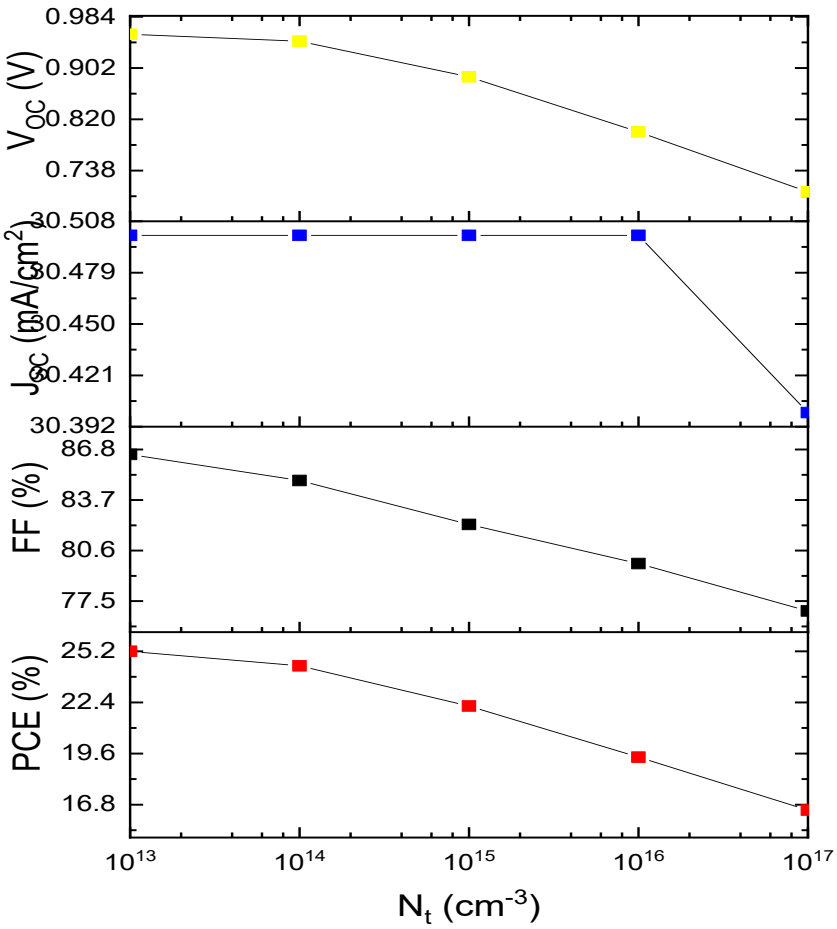


Figure 7. Plots of PCE, FF, $V_{OC,}$ and J_{SC} at various defect densities of the absorber layer

4.4. Effect of Device Operating Temperature

The influence of operating temperature on the performance of the $MASnI_3$-based inverted planar perovskite solar cell (IPSC) was investigated to determine the optimal thermal conditions for device operation. Table 6 summarizes the variation of key photovoltaic parameters with temperature, while Figure 8 illustrates the corresponding trends in J_{SC}, V_{OC}, PCE, and FF.

The simulation results indicate that increasing the operating temperature leads to a gradual decrease in V_{OC}, fill factor (FF), and power conversion efficiency (PCE), whereas the short-circuit current density (J_{SC}) remains largely unaffected. The relative stability of JSC can be attributed to

its weaker dependence on temperature-induced recombination, while the reductions in V_{OC}, FF, and PCE are primarily due to an increase in defect-assisted recombination at elevated temperatures (Slami et al., 2020). Additionally, several intrinsic material properties, including the band gap, carrier concentration, and electron and hole mobilities, are sensitive to temperature variations, which further contribute to the decline in device performance at higher temperatures(Al-Muhimeed et al., 2021)(M. Kumar et al., 2020). From the results, the highest PCE and FF of 22.2% and 82.2%, respectively, are achieved at 300 K, while the lowest values of 18.8% and 78.0% are observed at 360 K. These results align with prior research findings documented in the literature on $MASnI_3$-based IPSCs using Mg-TiO_2 as the ETL, which also identified near-ambient operating temperatures as optimal for maximizing device performance (Mallahasan & Onay, 2022; Usman & Bovornratanaraks, 2024).

Table 6. PV Characteristic parameter with the variation of temperature of the perovskite solar cell

Temperature(K)	PCE(%)	FF(%)	J_{SC}(mA/cm^2)	V_{OC}(V)
300	22.2	82.2	30.5	0.888
310	21.6	81.6	30.5	0.871
320	21.1	80.9	30.5	0.855
340	19.9	79.4	30.5	0.822
350	19.3	78.7	30.5	0.805
360	18.8	78.0	30.5	0.788

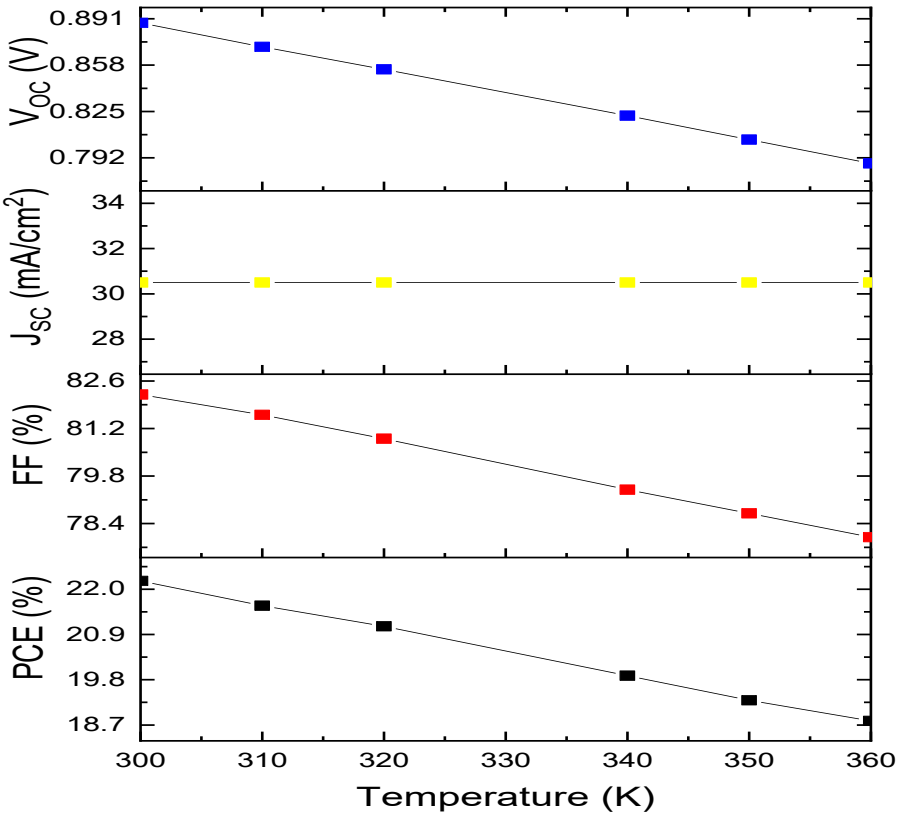


Figure 8. Plots of PCE, FF, J_{SC}, and V_{OC} against the temperature of the IPSC

4.5. Effect of Hole Transport Layer (HTL) Thickness on IPSC

The thickness of the hole transport layer (HTL) is one of the key design parameters influencing charge extraction efficiency, series resistance, and recombination dynamics in inverted planar perovskite solar cells (Danladi et al., 2023). In this investigation, the thickness of the Cu_2O HTL was systematically altered between 0.04 µm and 0.10 µm, while maintaining constancy in all other device parameters, to assess its impact on the performance of the device. The resulting photovoltaic characteristics are compiled in Table 7, and the graphical representations of JSC, V_{OC}, PCE, and FF as a function of HTL thickness are illustrated in Figure 9.

As illustrated in Table 7, both the PCE and the JSC exhibit a gradual decline with increasing thickness of the HTL, while the FF remains relatively stable. Specifically, JSC decreases from 30.8 mA cm^{-2} to 29.4 mA cm^{-2} as the HTL thickness increases. This reduction can be ascribed to

increased carrier recombination and transport losses within a thicker HTL layer. Similar reductions in current density with increasing transport layer thickness have also been reported in previous studies (Mallahasan & Onay, 2022).

A corresponding decline in PCE is observed, decreasing from 22.2% at an HTL thickness of 0.04 µm to 21.50% at 0.10 µm. This decrease is primarily associated with the reduction in JSC and the slight changes in FF as the HTL becomes thicker. These findings are in alignment with previous observations of (Oni et al., 2024), who reported that excessively thick transport layers introduce additional resistive losses and hinder efficient charge extraction.

Meanwhile, a slight increase in the open-circuit voltage (V_{OC}) is observed, rising from 0.877 V at 0.04 µm to approximately 0.890 V at HTL thicknesses up to about 0.06 µm, after which it remains nearly constant. The initial improvement in VOC can be attributed to improved surface coverage and enhanced hole selectivity at moderate HTL thicknesses, which helps suppress interfacial recombination at the $Cu_2O/MASnI_3$ interface. Once complete coverage is achieved and recombination is minimized, further increases in HTL thickness have little effect on recombination dynamics, resulting in a saturation of V_{OC}.

The trends illustrated in Figure 9 indicate that although a minimum HTL thickness is necessary to ensure complete surface coverage and effective hole extraction, excessive thickness can negatively affect device performance. In this study, the optimal HTL thickness lies within the range of 0.04–0.06 µm, where the device achieves the highest PCE and FF while maintaining relatively high V_{OC} and JSC. This optimal range represents a balance between minimizing series resistance and ensuring sufficient interfacial passivation and charge selectivity, which is consistent with previously reported optimal HTL thicknesses for inverted perovskite solar cells (Ogunmoye et al., 2025).

Table 7. J-V Characteristic parameter with the variation of the thickness of the HTL of the perovskite device

Thickness(µm)	PCE(%)	FF(%)	J_{SC}(mA/cm^2)	V_{OC}(V)
0.04	22.2	82.0	30.8	0.877
0.05	22.2	82.2	30.5	0.888

0.06	22.1	82.2	30.2	0.890
0.07	21.9	82.2	30.0	0.891
0.08	21.8	82.2	29.8	0.891
0.09	21.7	82.2	29.6	0.891
0.10	21.5	82.2	29.4	0.891

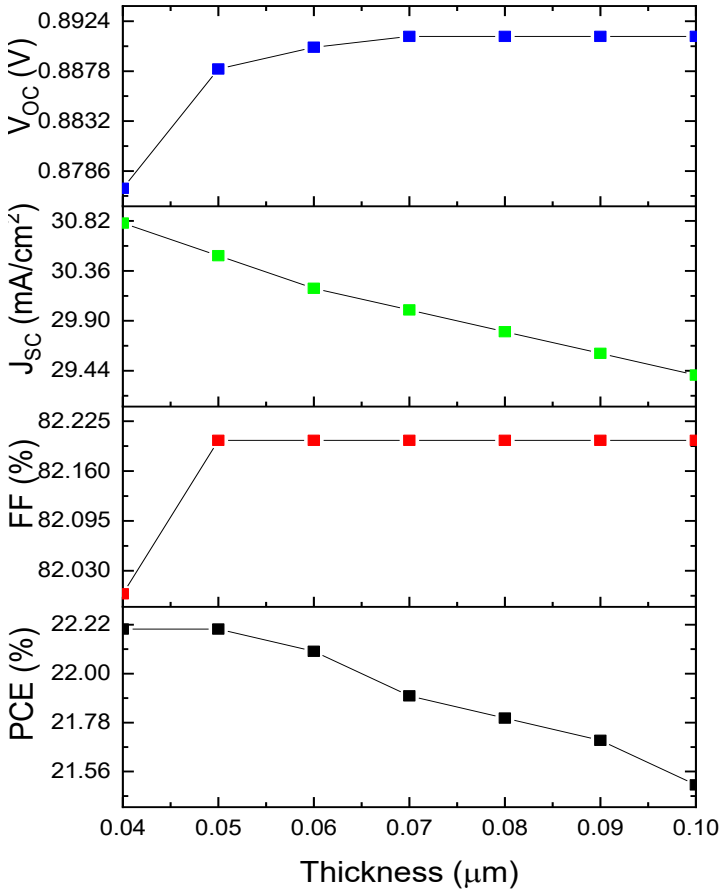


Figure 9. Plots of PCE, FF, J_{SC}, and V_{OC} with variation of HTL thickness of the IPSC

4.6 Comparison with Previous Studies

As far as we are aware, experimental results for the exact device configuration FTO/Cu_2O/$CH_3NH_3SnI_3$/Mg-TiO_2/Ag have not yet been reported in the literature. This absence

makes the present study both novel and significant. The limited experimental realization of this structure may be attributed to challenges such as the relatively high processing temperatures required for some of the inorganic layers and the comparatively with the all-inorganic transport materials utilized in nano-electronic devices exhibit reduced electrical conductivity in comparison to the widely employed organic transport materials.

Nevertheless, several simulation studies involving similar material combinations have been reported. For instance, investigations based on the n–i–p device architecture by (Danladi et al., 2022)(Mallahasan & Onay, 2022)(Mottakin et al., 2021) reported PCEs of 15.10%, 21.94%, and 24.45%, respectively. In addition, simulation studies employing the p–i–n configuration by (A. Kumar et al., 2021),(Nyiekaa et al., 2024) reported higher efficiencies of 27.43% and 30.1%, respectively, as summarized in Table 8.

The findings produced in this study align with those documented in prior research. studies, further validating the reliability of the proposed model and highlighting the potential of the FTO/Cu_2O/$CH_3NH_3SnI_3$/Mg-TiO_2/Ag structure for high-performance lead-free perovskite solar cells.

Table 8. Photovoltaic parameters of Sn-based perovskite solar cells of some reported simulated works from the literature.

Device structure	Parameters				Study type	Reference
HTM/Absorber/ETM	V_{OC}(V)	J_{SC}(mAcm^{-2})	FF(%)	PCE(%)		
CuO/$CH_3NH_3SnI_3$/ZnO	0.830	29.71	61.30	15.1	Simulation	(Danladi et al., 2022)
Cu_2O/$CH_3NH_3SnI_3$ /TiO_2	0.865	29.96	84.62	21.94	Simulation	(Mallahasan & Onay, 2022)
Cu_2O/$CH_3NH_3SnI_3$ /ZnO	1.0867	33.49	82.88	30.17	Simulation	(Nyiekaa et al., 2024)

HTM-free/$CH_3NH_3PbI_3$/ Li-TiO_2	1.011	22.54	69.98	I5.94	Simulation	(Danladi et al., 2023)
Spiro-omeTAD /$CH_3NH_3PbI_3$/Mg-TiO_2	1.170	23.17	72.74	15.95	Simulation	(Usman & Bovornratanaraks, 2024)
Cu_2O/$CH_3NH_3SnI_3$ /TiO_2	1.203	25.97	87.79	27.43	Simulation	(A. Kumar et al., 2021)
Cu_2O/$CH_3NH_3SnI_3$/Mg-TiO_2	0.9786	33.58	87.85	28.88	Simulation	This work

5. Conclusions

In this study, an extensive numerical analysis of $MASnI_3$-based inverted planar perovskite solar cells was conducted utilizing the SCAPS-1D simulation framework. The effects of critical device parameters—such as the thickness of the absorber layer, thickness of the hole transport layer, density of defects within the absorber, concentration of acceptor doping, operational temperature, and resistive losses were rigorously examined to elucidate their influence on the photovoltaic efficacy of the device.

The simulation results reveal that device performance is strongly dependent on the optimization of these parameters. In particular, a moderately thick absorber layer, an optimized HTL thickness, low bulk defect density, near-ambient operating temperature, and reduced series resistance were found to be critical for achieving high efficiency and stable operation in lead-free perovskite solar cells. These factors significantly influence charge generation, transport, and recombination processes within the device.

The optimized device structure yielded a PCE of 28.88%, with an open-circuit voltage (V_{OC}) of 0.9786 V, a J_{SC} of 33.58 mA/cm², and an FF of 87.85%. These results demonstrate the strong potential of $MASnI_3$-based inverted planar perovskite solar cells for high-performance photovoltaic applications. Although the simulated efficiency is high, it represents an ideal scenario

under controlled assumptions. Practical devices may exhibit lower efficiencies due to Sn^{2+} oxidation, interface defects, and fabrication constraints."

Despite these promising findings, several challenges remain for practical implementation. In particular, reducing defect density and improving the stability of Sn^{2+} in the absorber layer remain critical issues that require further investigation. Advances in fabrication techniques, material engineering, and interface optimization are expected to address these limitations.

Overall, the insights obtained from this study provide valuable design guidelines for the development and experimental realization of efficient, stable, and environmentally friendly $MASnI_3$-based inverted planar perovskite solar cells.

Authors' contributions:

Linus Friday Apeh: Conceptualization, Methodology, Writing – Original Draft, Formal Analysis, Validation Software, Investigation,

Jonathan Terseer Ikyumbur: Conceptualization, Supervision, writing – Original Draft, Formal analysis, Project Administration, Investigation, Writing – Original Draft, Validation,

Frederick Gbaorun: Resources, Supervision, Writing – Review & Editing

Raymond Msughter Agaku: Writing – Review & Editing

Ode Samuel Omenka: Writing – Review & Editing

Funding: The authors declare that no specific funding was received for this work.

Conflicts of Interest: The authors declare no competing interests.

Data Availability: The data supporting the findings of this study will made available upon request

References

Abate, A. (2023). *Stable Tin-Based Perovskite Solar Cells*. 8–11. https://doi.org/10.1021/acsenergylett.3c00282

Al-Muhimeed, T. I., Shafique, A., AlObaid, A. A., Morsi, M., Nazir, G., AL-Anazy, M. mana, & Mahmood, Q. (2021). New lead-free double perovskites X2GeI6 (X = K, Rb, Cs) for solar cells, and renewable energy as an alternate of hybrid perovskites. *International Journal of Energy Research*, *45*(13), 19645–19652. https://doi.org/10.1002/er.7022

Bouderbala, I. Y., & Hamdi, N. H. (2023). *291-Article Text-1524-1-10-20230617*. *08*, 131–137.

Chowdhury, T. A., Bin Zafar, M. A., Sajjad-Ul Islam, M., Shahinuzzaman, M., Islam, M. A., & Khandaker, M. U. (2023). Stability of perovskite solar cells: issues and prospects. *RSC Advances*, *13*(3), 1787–1810. https://doi.org/10.1039/D2RA05903G

Danladi, E., Gyuk, P. M., Tasie, N. N., Egbugha, A. C., Behera, D., Hossain, I., Bagudo, I. M., Madugu, M. L., & Ikyumbur, J. T. (2023). Impact of hole transport material on perovskite solar cells with different metal electrode: A SCAPS-1D simulation insight. *Heliyon*, *9*(6), e16838. https://doi.org/10.1016/j.heliyon.2023.e16838

Danladi, E., Salawu, A. O., Abdulmalik, M. O., Onoja, E. D., Onwoke, E. E., & Adepehin, D. S. (2022). Optimization of Absorber and ETM Layer Thickness for Enhanced Tin based Perovskite Solar Cell Performance using SCAPS-1D Software. *Physics Access*, *02*(01), 1–11. https://doi.org/10.47514/phyaccess.2022.2.1.001

Durodola, O. M., Ugwu, C., & Danladi, E. (2023). Highly efficient lead-free perovskite solar cell based on magnesium-doped copper delafossite hole transport layer: a SCAPS-1D framework prospect. *Emergent Materials*, *6*(5), 1665–1684. https://doi.org/10.1007/s42247-023-00542-8

Fan, Y., Wu, Y., Xu, Y., Li, W., Zhou, H., & Zhang, X. (2022). Situation and Perspectives on Tin-Based Perovskite Solar Cells. *Sustainability (Switzerland)*, *14*(24). https://doi.org/10.3390/su142416603

Gholami-Milani, A., Ahmadi-Kandjani, S., Olyaeefar, B., & Kermani, M. H. (2023). Performance analyses of highly efficient inverted all-perovskite bilayer solar cell. *Scientific Reports*, *13*(1), 1–15. https://doi.org/10.1038/s41598-023-35504-x

Islam, R., Rumel, M. H., & Alam, K. (2024). *Numerical Analysis and HTL Variation of*

CH3NH3SnI3 Based Perovskite Solar Cell Using. *8*(9), 83–87.

Kumar, A., Srivastava, S., Mahapatra, A., & Kumar, J. (2021). Performance optimization of lead free-MASnI 3 based solar cell with 27 % efficiency by numerical simulation. *Optical Materials*, *117*(May), 111193. https://doi.org/10.1016/j.optmat.2021.111193

Kumar, M., Kumar, A., Raj, A., Chandra, P., & Sahni, M. (2020). Materials Today : Proceedings Organic-inorganic perovskite-based solar cell designs for high conversion efficiency : A comparative study by SCAPS simulation. *Materials Today: Proceedings*, *xxxx*. https://doi.org/10.1016/j.matpr.2020.11.035

Li, X., Zhang, W., Guo, X., Lu, C., Wei, J., & Fang, J. (2022). Constructing heterojunctions by surface sulfidation for efficient inverted perovskite solar cells. *Science*, *375*(6579), 434–437. https://doi.org/10.1126/science.abl5676

Mallahasan, H., & Onay, Ö. (2022). *Investigation of the Effect of Different Factors on the Performance of Several Perovskite Solar Cells : A Simulation Study by SCAPS*. *5*, 20–38.

Mottakin, M., Sobayel, K., Sarkar, D., Alkhammash, H., Alharthi, S., Techato, K., Amin, N., & Sopian, K. (2021). *Design and Modelling of Eco-Friendly CH 3 NH 3 SnI 3 -Based Perovskite Solar Cells with Suitable Transport Layers*.

Nyiekaa, E. A., Aika, T. A., Danladi, E., Akhabue, C. E., & Orukpe, P. E. (2024). Simulation and optimization of 30.17% high performance N-type TCO-free inverted perovskite solar cell using inorganic transport materials. *Scientific Reports*, *14*(1), 1–17. https://doi.org/10.1038/s41598-024-62882-7

Nyinongo, G. T., Ikyumbur, J. T., Gbaorun, F., Aper, T. M., & Danladi, E. (2025). Numerical Analysis of the Absorber Layer of Perovskite Solar Cells based on Cu2O as Hole Transporting Material. *Journal of Energy Research and Reviews*, *17*(1), 52–65. https://doi.org/10.9734/jenrr/2025/v17i1392

Obada, D. O., Muhammad, M., Tajiri, S. B., Kekung, M. O., Abolade, S. A., Akinpelu, S. B., & Akande, A. (2024). A review of renewable energy resources in Nigeria for climate change mitigation. *Case Studies in Chemical and Environmental Engineering*, *9*, 100669. https://doi.org/10.1016/j.cscee.2024.100669

Ogunmoye, K. A., Izang, J. C., Olorunyolemi, I., & Ozurumba, A. C. (2025). *Highly efficient MAGeI 3 HTL-free perovskite solar cell with lithium-doped electron transport layer : A dive into SCAPS-1D simulation insight*. *7*(2), 34–50.

Oni, A. M., Mohsin, A. S. M., Rahman, M. M., & Hossain Bhuian, M. B. (2024). A comprehensive evaluation of solar cell technologies, associated loss mechanisms, and efficiency enhancement strategies for photovoltaic cells. *Energy Reports*, *11*, 3345–3366. https://doi.org/10.1016/j.egyr.2024.03.007

Patel, P. K. (2021). Device simulation of highly efficient eco - friendly - perovskite solar cell. *Scientific Reports*, 1–11. https://doi.org/10.1038/s41598-021-82817-w

Prasangi, M., & Srilalitha, M. D. V. (2025). *Temperature-Dependent Performance Analysis of Lead- Free MASnI ₃ Perovskite Solar Cells with Cu ₂ O and SnO ₂ Transport Layers*. *21*(3), 207–212.

Rengifo-Herrera, J. A., Osorio-Vargas, P., & Pulgarin, C. (2022). A critical review on N-modified TiO2 limits to treat chemical and biological contaminants in water. Evidence that enhanced visible light absorption does not lead to higher degradation rates under whole solar light. *Journal of Hazardous Materials*, *425*, 127979. https://doi.org/10.1016/J.JHAZMAT.2021.127979

Ru, P., Bi, E., Zhang, Y., Wang, Y., Kong, W., & Sha, Y. (2020). *High Electron Affinity Enables Fast Hole Extraction for Efficient Flexible Inverted Perovskite Solar Cells*. *1903487*, 1–9. https://doi.org/10.1002/aenm.201903487

Sharif, R., Khalid, A., Ahmad, S. W., Rehman, A., Qutab, H. G., Akhtar, H. H., Mahmood, K., Afzal, S., & Saleem, F. (2023). A comprehensive review of the current progresses and material advances in perovskite solar cells. *Nanoscale Advances*, *5*(15), 3803–3833. https://doi.org/10.1039/D3NA00319A

Sumona, F. B., Kashif, M., Danladi, E., Tighezza, A. M., Al-Mahmud, N., Toki, G. F. I., Pandey, R., & Hossain, M. K. (2023). Optimization of Perovskite-KSnI3 Solar Cell by Using Different Hole and Electron Transport Layers: A Numerical SCAPS-1D Simulation. *Energy and Fuels*, *37*(23), 19207–19219. https://doi.org/10.1021/acs.energyfuels.3c02397

Sumona, F. B., Kashif, M., Madan, J., Metwally, A. S. M., Danladi, E., & Nahid-Al-Mahmud. (2024). Optimization of lead-free KSnI3 perovskite solar cell by numerical simulation with enhanced efficiency of 20.34%. *Journal of Optics (India)*. https://doi.org/10.1007/s12596-024-02158-5

Totolhua, E. P., Ben, A., Leyva, K. M., Piñ, A. C., Flores-m, J., & Luna, A. (2023). *Numerical Simulation of an Inverted Perovskite Solar Cell Using a SiOx Layer as Down-Conversion*

Energy Material to Improve Efficiency and Stability.

Usman, A., & Bovornratanaraks, T. (2024). Modeling and Optimization of Modified TiO2 with Aluminum and Magnesium as ETL in MAPbI3 Perovskite Solar Cells: SCAPS 1D Frameworks. *ACS Omega*. https://doi.org/10.1021/acsomega.4c04505

Valadi, K., Gharibi, S., Taheri-Ledari, R., Akin, S., Maleki, A., & Shalan, A. E. (2021). Metal oxide electron transport materials for perovskite solar cells: a review. *Environmental Chemistry Letters*, *19*(3), 2185–2207. https://doi.org/10.1007/s10311-020-01171-x

Zhou, H., Wang, H., Yue, C., He, L., Li, H., Zhang, H., Yang, S., & Ma, T. (2024). Photocatalytic degradation by TiO2-conjugated/coordination polymer heterojunction: Preparation, mechanisms, and prospects. *Applied Catalysis B: Environment and Energy*, *344*, 123605. https://doi.org/10.1016/J.APCATB.2023.123605

Supplementary Files

This is a list of supplementary files associated with this preprint. Click to download.

- CRediTAuthorStatement.docx
- Declarationofinterestsstatement.docx